JACS
JOURNAL OF THE AMERICAN CHEMICAL SOCIETY

Article

Influence of spatial distribution of cationic functional groups at nanoparticle surfaces on bacterial viability and membrane interactions

Yongqian Zhang, Natalie V. Hudson-Smith, Seth D. Frand, Meghan S Cahill, Larissa S. Davis, Z. Vivian Feng, Christy L. Haynes, and Robert J Hamers

J. Am. Chem. Soc., **Just Accepted Manuscript** • DOI: 10.1021/jacs.0c02737 • Publication Date (Web): 13 May 2020

Influence of spatial distribution of cationic functional groups at nanoparticle surfaces on bacterial viability and membrane interactions

Yongqian Zhang[†], Natalie V. Hudson-Smith[‡], Seth D. Frand[⊥], Meghan S. Cahill[‡], Larissa S. Davis[†§], Z. Vivian Feng[⊥], Christy L. Haynes[‡], Robert J. Hamers[†*]

[†]University of Wisconsin-Madison, Department of Chemistry, Madison, WI 53706, USA

[‡]University of Minnesota Twin Cities, Department of Chemistry, Minneapolis, MN 55455, USA

[⊥]Augsburg University, Department of Chemistry, Minneapolis, MN 55454, USA

ABSTRACT: While positively charged nanomaterials induce cytotoxicity in many organisms, much less is known about how the spatial distribution and presentation of molecular surface charge impacts nanoparticle-biological interactions. We systematically functionalized diamond nanoparticle surfaces with five different cationic surface molecules having different molecular structures and conformations, including four small ligands and one polymer, and we then probed the molecular-level interaction between these nanoparticles and bacterial cells. *Shewanella oneidensis* MR-1 was used as a model bacterial cell system to investigate how molecular length and conformation of cationic surface charges influence their interactions with the Gram-negative bacterial membranes. Nuclear magnetic resonance (NMR) and X-ray photoelectron spectroscopy (XPS) demonstrate the covalent modification of nanoparticle surface with the desired cationic organic monolayers. Surprisingly, bacterial growth-based viability (GBV) and membrane damage assays both show only minimal biological impact by the NPs functionalized with short cationic ligands within the concentration range tested. Yet NPs covalently linked to a cationic polymer induce strong cytotoxicity, including reduced cellular viability and significant membrane damage at the same concentration of cationic groups. Transmission electron microscopy (TEM) images of these NP-exposed bacterial cells show that NPs functionalized with cationic polymers induce significant membrane distortion and production of outer membrane vesicles, while NPs bearing short cationic ligands exhibit only weak membrane association. Our results demonstrate that the spatial distribution of molecular charge plays a key role in controlling the interaction of cationic nanoparticles with bacterial cell membranes and subsequent biological impact. Nanoparticles functionalized with ligands having different lengths and conformations can have large differences in interactions even while having nearly identical zeta potentials. While zeta potential is a convenient and commonly used measure of nanoparticle charge, it does not capture essential differences in molecular-level nanoparticle properties that control their biological impact.

INTRODUCTION

The surface chemistry of nanoparticles (NPs) plays a key role in controlling the interactions of nanoparticles with each other and with their surroundings.[1-11] The intentional functionalization of nanoparticles with molecular coatings such as short-chain ligands or polymeric coatings provides one approach to controlling their environmental and biological impacts.[3, 5-10]

Prior studies have frequently reported that nanoparticles with cationic functional groups interact more strongly with bacterial cells compared with those functionalized with neutral or negatively charged groups,[3, 5, 7, 9, 12] These differences have frequently been attributed to the favorable electrostatic interactions between positively charged NP surfaces and negatively charged cell membranes.[2-3, 10, 12] NPs with cationic surfaces generally show higher cell-membrane affinity and penetration compared to anionic and neutral surfaces,[2, 12-15] and NPs with higher surface charge density lead to higher bacterial toxicity and membrane permeability.[16-17]

While the impact of cationic surface functional groups on nanoparticle-cell interactions is widely recognized as important, much less is known about how the molecular conformation of surface ligands and the resulting spatial distribution of charge affect their resulting biological impact. Prior studies have shown that differences in the arrangement of surface ligands can impact the ability of nanoparticles to penetrate cell membranes,[8, 16-18] suggesting the importance of NP surface ligand conformation to membrane interactions. One challenge with understanding the influence of surface molecular layers is that self-assembled monolayers on gold and most other nanoparticles of interest can be easily removed or displaced under biological conditions.[19-21] Nanodiamond is an excellent platform for understand the influence of surface

molecular groups because functionalization via an "all-carbon" scaffold provides outstanding stability.[22-25] In prior work using nuclear magnetic resonance (NMR) T_2 measurements, we found that when a model cationic polymer was covalently linked to diamond nanoparticles, approximately 45 % of the segments are highly mobile, while the rest (~55 %) remain tightly bound on the NP surfaces.[26] In contrast, nanoparticles functionalized with short molecular linkers must have the charged groups closer to the surface.

Here, we demonstrate how the spatial distribution of charged molecular functional groups at the surface of diamond nanoparticles impacts their interactions with a Gram-negative model bacterium. Figure 1 shows the five cationic diamond NP surfaces that we prepared, using an approach we described previously.[25] To identify the influence of primary vs. quaternary amino groups, we prepared diamond nanoparticles (DNPs) linked via 3-carbon chains to terminal primary amino groups (C3-NH_3^+-DNPs) and quaternary (tetramethylammonium) amino groups (C3-$N(CH_3)_3^+$-DNPs. To explore the influence of chain length we also prepared DNPs with a C11 chain terminated with tetramethylammonium group (C11-$N(CH_3)_3^+$-DNPs). To determine the influence of charges distributed along the length of the molecules we prepared DNPS functionalized with tetraethylenepentamine (TEPA-DNPs). Finally, to determine the influence of ligand conformational flexibility, we synthesized DNPS with a covalently bonded poly(allylamine) (PAH-DNPs). We use *Shewanella oniedensis* MR-1 (*S. oneidensis*) as a model biological organism due to its ubiquity and importance in the environment.[27-28] Previous studies have shown *S. oneidensis* to be more hardy than other Gram-negative bacteria models, signifying that any impacts measured here are likely to be amplified in other strains. In addition, working with *S. onidensis* MR-1 allows comparison to other studies, including those with ligands similar to those studies here.[29]

Using the above surface modifications, we employed a bacterial Live/Dead (L/D) assay, a growth-based viability (GBV) assay, and transmission electron microscopy (TEM) to characterize how nanoparticles functionalized with these molecules interacted with *Shewanella*. Our results show that PAH-DNPs induce high cytotoxicity by disrupting the integrity of bacterial cell membranes. Surprisingly, however, the nanoparticles functionalized with shorter linear molecules all exhibited only weak association with bacterial cell membranes and little toxicity, even though their measured zeta potentials are similar to that of the PAH-modified nanoparticles. While zeta potential is a convenient and commonly used measure of nanoparticle charge, it does not capture essential differences in molecular-level nanoparticle properties that control their biological impact. Our results suggest that the presence of conformationally flexible molecular groups extending away from the nanoparticle core and therefore able to intercalate into the outer molecular layers of bacterial cell membranes is a key molecular factor controlling biological impact of cationic functionalized nanoparticles.

Experimental Section

Materials. All reagents were purchased from Sigma-Aldrich, unless noted otherwise. Nanopure water (resistivity ≥18 MΩ ・cm, Thermo Scientific Nano-pure system GenPure UV-TOC/UF xCAD plus) was used for all experiments. The terminal alkenes used to functionalize diamond nanoparticles (DNPs) in this paper are allyl trimethylammonium bromide, *tert*-Butyl *N*-allylcarbamate (98%), 11-trimethylammonium-1-undecene bromide and 5-hexenoic acid (98%). Allyl trimethylammonium bromide was synthesized by a reported method;[25] and 11-trimethylammonium-1-undecene bromide was synthesized by a modified procedure.[30] See Supporting Information for detailed synthesis procedures and ^{1}H NMR and ^{13}C NMR (Supporting Information, S1). Both allyl trimethylammonium bromide and 11-trimethylammonium-1-undecene bromide absorb moisture over time to form insoluble complex, thus need to be stored in a moisture-free environment.

Preparation of different positively charged diamond nanoparticle surfaces. Detonation diamond nanoparticles (5 nm average primary particle size, Nanostructured & Amorphous Material Inc.) (DNPs) were used for studies reported here. These DNPs were functionalized with five different positively charged ligands using a radical-based method we reported previously.[25] Figure 1 shows an overview of the functionalization process and the chemical structures of the five different positively charged DNP surfaces. The DNPs were heated in a tube furnace with a flow of pure hydrogen gas (1 atm, 50 standard cm^3 min^{-1}) at 600 °C for 6 h to hydrogen-terminate the surface atoms.[25, 31] The TEM micrographs of the hydrogenated- DNPs from our previous study show an average core particle size of 5 nm

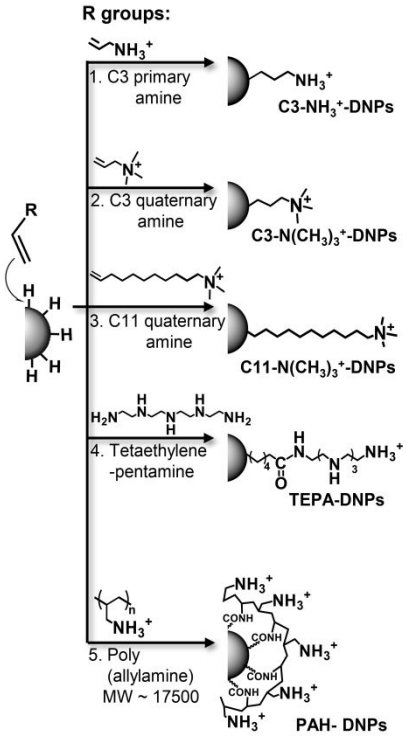

Figure 1. Functionalization scheme of five cationic amine-containing monolayer binding to 5 nm-core hydrogen-functionalized diamond nanoparticles (DNPs). Molecules and DNPs are not drawn to scale.

and no evidence for graphitic shells.[25] The reactant solution containing benzoyl peroxide (Luperox A98, >98%), the reactant molecule of interest, and an appropriate anhydrous solvent were very briefly (~10 min) dried over 3 Å molecular sieves to help sequester any water present in the benzoyl peroxide. The supernatant was removed, mixed with hydrogen-terminated DNPs, and heated at 80 ^{0}C for 3.5 h while stirring under an argon atmosphere. The solution was cooled slowly to room temperature overnight. Details of the conditions used for functionalizing these five surfaces are included in Supporting information (S2). The functionalized DNPs were purified by rinsing in the corresponding reaction solvent (50 mL per 50 mg DNPs) with sonication to ensure resuspension, followed by centrifugation at 4480 g (gravitational constant) until the samples fully pellet (typically 5-50 min). The washing and centrifugation steps were repeated with water (50 mL per 50 mg DNPs, 1x). The final samples were resuspended in 1 mM HCl solution and centrifuged at 14400 g for 30 mins. Aggregated NPs were removed, leaving behind individual NPs and small clusters for biological studies.

Characterization of diamond NPs surfaces. We measured the hydrodynamic diameters and zeta potentials of the functionalized DNPs using dynamic light scattering (DLS) and electrophoretic light scattering (Marvern Zetasizer ZS). The results from these measurements is provide in the Supporting Information (S3). In summary, the average hydrodynamic diameter of all five types of nanoparticles after functionalization is 41.0 nm, and the average zeta potential is + 42.7 mV. Chemical compositions and surface structures of all functionalized diamond nanoparticles were characterized by both X-ray photoelectron spectroscopy (XPS) and nuclear magnetic resonance (NMR). X-ray photoelectron spectroscopy (XPS) measurements were performed using Thermo Scientific K-alpha XPS system with a micro-focused monochromated Al Kα X-ray source and 180° hemispherical analyzer with a 128-channel detector using and analyzer pass energy of 50 eV. XPS data were analyzed using Casa XPS software[32] and were energy-referenced to the C(1s) peak at 284.8 eV binding energy. Samples for XPS were prepared by drop-casting 20 μL of a dilute sample onto doped silicon wafers (B-doped, 0.1-1 ohm·cm resistivity, Electro-Optic Materials). NMR measurements were performed using a Bruker Avance-600 spectrometer with TCI-F cryoprobe. To ensure quantitative results, the recycling time (d1) was set to 10 s, which is more than 5 times longer than the T_1 of the protons of interest. Large solvents peaks were reduced in intensity using solvent suppression to achieve high-quality data. DNPs samples for NMR analysis were further centrifuged down (14100 *g*) to form pellets and re-dissolved in D_2O. This process replaced H_2O with D_2O as much as possible and was repeated at least 3 times. The samples were then further disaggregated with sonication.

Evaluation of toxicity toward bacteria: To evaluate the toxicity of five different cationic functionalized DNPs, we used a growth-based viability (GBV) assay.[33] *Shewanella oneidensis* MR-1 (*S. oneidensis*) were grown from stock solution that was stored in 30% glycerol at -80 °C; the bacteria were inoculated into Luria-Bertani broth (LB) agar plates and incubated at 30 °C for 18-24 h. The resulting bacterial colonies were inoculated into 10 mL LB broth and incubated at 30°C for 4-6 h or until midlog phase. These cultures were centrifuged at 750 g for 10 min and resuspended with 1x Dulbecco's phosphate buffered saline (DPBS) (Corning) for 10 min. This DPBS solution was centrifuged again at 750 g for 10 minutes and resuspended in HEPES buffer (2 mM, pH 7.4) to obtain a concentration with an optical density of 0.1 at 600 nm. In this study, we normalize nanoparticle doses based on the total amine concentration of the surrounding ligands, as described below. In a 96-well plate, aliquots of *Shewanella* were introduced, followed by addition of functionalized DNPs to achieve amine concentrations (after dilution) of 1.24, 2.5, 5, 10, 20, 40 and 80 nM. After 1 h of exposure, 5-μL aliquot was removed from each of the 96 wells and added to 195 μL of fresh LB broth in triplicate and optical density readings were collected with a BioTek Synergy Mx Microplate Reader at 600 nm every 20 min over the course of 19 h at 30 °C and with medium intensity agitation for 1 min prior to each reading. Growth curves were analyzed as described previously.[33]

Bacterial Live/Dead Assay (L/D assay). The LIVE/DEAD® BacLight™ Viability Kit (ThermoFisher Scientific) was used to quantify bacterial membrane damage by different cationic DNPs. *S. oneidensis* suspensions were prepared and cultured. Functionalized DNPs were introduced into the suspensions at concentrations identical to those used in GBV measurements. Samples were then distributed in a 96-well plate in at least triplicate and were exposed to a stain consisting of a mixture of SYTO 9 dye and propidium iodide for 15 min following the manufacturer's recommendations. Briefly, fluorescence measurements were performed using a plate reader (BioTek Synergy Mx Microplate Reader) with excitation wavelength of 485 nm and emission at 528 nm (for SYTO9 stain) and 638 nm (for propidium iodide stain). The ratio of fluorescence intensities at 528 nm and 638 nm, I_{528}/I_{638}, was compared with that of control samples of live and dead bacteria, yielding an average fraction of bacteria with intact membranes (live bacteria). The bacterial viability assay is based on growth rates of nanoparticle-exposed bacterial populations compared with growth of control populations. Experimental variations between bacterial populations can yield individual measurements with calculated viability slightly greater than 100%; however, replicate measurements show that none of the measurements exceed 100% viability in a statistically significant manner.

Transmission Electron Microscopy (TEM). Transmission electron microscopy (TEM) images of *S. oneidensis* MR-1 exposed to nanodiamonds were obtained with a FEI Tecnai T12 with a 120-kV operating voltage after resin embedding. *S. oneidensis* MR-1 that were exposed to functionalized DNPs were washed in D-PBS and suspended in HEPES buffer. The exposed bacteria suspension was centrifuged down to a pellet, washed 3x with 0.1 M cacodylate buffer, and fixed for 50 minutes in 2.5% glutaraldehyde in 0.1 M sodium cacodylate buffer. Fixed cell pellets were washed with sodium cacodylate buffer, dehydrated with increasing concentrations of ethanol solutions (30, 50, 70, 80, 90, 95, 100% EtOH in water), and rinsed with propylene oxide three times. Then, the pellets were soaked in a 2:1 propylene oxide/epoxy resin for two

hours, 1:1 propylene oxide/epoxy resin overnight, fresh 1:1 propylene/epoxy resin for 5 hours, and then finally fixed in pure resin for in a vacuum oven. Slices of the pellet were microtomed with a Leica uC6 microtome for imaging. Sections were stained with uranyl acetate and lead citrate and placed on copper TEM grids (Ted Pella Inc) for imaging.

Normalization of *S. oneidensis* responses to amine concentration. While biological responses to nanomaterials are frequently plotted using nanoparticle concentrations as an experimental variable, our work is aimed at understanding the effect of the charge amino functional groups. The number of amino groups per nanoparticle varies with the identity of the ligand. For example, nanoparticles functionalized with small molecule ligands bearing a single amino group present a smaller number of amino groups compared with DNPs functionalized with cationic polymers. Therefore, to understand if this inherently higher amine content in PAH-DNPs contributes to the significantly higher membrane damage and cytotoxicity, we analyzed the responses of GBV and L/D assay using the total concentration of exposed amine groups in each sample. We used quantitative ^{1}H NMR to determine the total concentration of amine moieties in each sample and normalized the GBV toxicity and L/D membrane damage to yield the resulting biological impact for a given concentration of amino groups. This normalization allows us to compare the bio- responses to per amine among different DNP surfaces. For quantitative NMR analysis, three known amounts of each propylamine (with D_2O), propyl trimethylamine (with D_2O), 11-trimethylamine (with D_2O), tetraethylenepentamine (with D_2O) and poly(allylamine) (with D_2O) were used as external standards, and peak integrations were compared to these standards. Relaxation delay was set to at least 5 times the T_1 of the standards and integrated peak areas are normalized with the number of scans and the receiver gain.

RESULTS

Characterization of functionalized DNPs. In order to verify that the DNPs are functionalized as expected, we characterized the functionalized DNDs using x-ray photoelectron spectroscopy (XPS). Figures 2a-e show the N(1s) spectra for all five different cationic surfaces: polyallylamine hydrochloride-DNPs (PAH-DNPs, Fig. 2a), tetraethylenepentamine-DNPs (TEPA-DNPs, Fig. 2b), C3 primary amine-DNPs (C3-NH_3^+-DNPs, Fig. 2c), C3 quaternary amine-DNPs (C3-$N(CH_3)_3^+$-DNPs, Fig. 2d) and C11 quaternary amine-DNPs (C11-$N(CH_3)_3^+$-DNPs, Fig. 2e). The nitrogen region for PAH-DNPs (Fig. 2f) shows two peaks at 399 eV and 401 eV. TEPA- DNPs (Fig. 2g) has two peaks at 399.6 eV and 401 eV. Nitrogen 1s peaks that are centered at 399-400 eV are often assigned as non-protonated amine moieties such as C-N, -NH_2;[34-35] while nitrogen peaks that are at higher binding energies (400 eV-402 eV) have been reported as amide bonds (-NH-CO) and amines that are in their protonate states (-NH_3^+, -$N(CH_3)_3^+$).[23, 34, 36] From our results shown in Fig. 2a-e, the amide bond moiety at 401 eV binding energy is only observed for PAH-DNPs and TEPA-DNPs, and is consistent with these surface structures because the PAH and TEPA molecules are linked to the carboxylate DNP surfaces through amide linkage. The N(1s) spectra of C3-NH_3^+-DNPs (Fig. 2c), C3- $N(CH_3)_3^+$-DNPs (Fig. 2d) and C11- $N(CH_3)_3^+$-DNPs (Fig. 2e) show two peaks that are centered at 399.6 eV and 402.2 eV, and are consistent with the C-N nitrogen (399.6 eV),[37] -NH_3^+ and -$N(CH_3)_3^+$ nitrogen (402.2 eV, protonated amines)[34-35] moieties that are present at these surfaces. Figures 2f-j show C(1s) spectra for all five cationic surfaces. The peak at 284.8 eV is present in all carbon 1s spectra and corresponds to C-C and C-H from diamond cores and hydrocarbon chains at DNP surfaces.[23] Peaks centered at 286 eV are also observed in all C(1s) spectra and are consistent with the C-N moieties that are present in all these surfaces. Nitrogen moieties such as C-N and C=N at carbon nanoparticle surfaces have been reported to appear at approximately 285.9 ± 0.1 eV.[25, 35] Additional peaks at 288.1 eV are observed in PAH-DNPs (Fig. 2f) and TEPA-DNPs (Fig. 2g). C(1s) spectra, which we attribute to C(1s) atoms in amide linkages[38] (N-C=O) resulting from the EDC coupling. The carbon 1s spectra show consistent results with the nitrogen spectra for each cationic DNP surfaces, which further verified the presence of C-N, CO-NH and -NH_2/NH^{3+} moieties in our samples. XPS measurements were done and quantified independently on both Si and Au substrates (drop-cast substrates) to verify data consistency. The line shapes of N(1s) and C(1s) were very consistent among measurements using different drop-case substrates and among replicates (Supporting Information S4). The XPS results in Figure 2 confirm that the DNP surfaces have been functionalized with different amine moieties through covalent bonds, yielding the structures shown in Fig. 1. Quantitative analysis of the XPS data (Supporting Information S5 for details) yields an average surface coverage of 0.7 ± 0.2 molecules per nm^2 for the DNPs functionalized with linear ligands, consistent with one monolayer coverage as previously reported.[25]

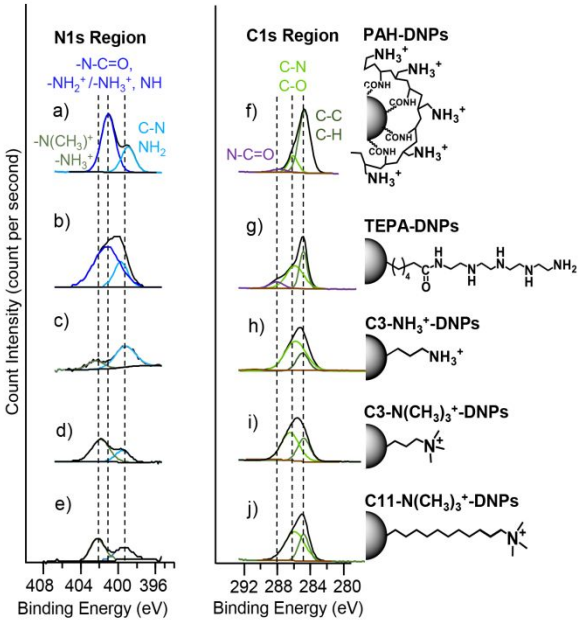

Figure 2. XPS spectra of N(1s) regions (a-e) and C(1s) regions (f-j) of PAH-DNPs, TEPA-DNPs, C3-NH3+-DNPs, C3-N(CH3)$_3^+$-DNPs and C11-N(CH_3)$_3^+$-DNPs.

Surface structural analysis using NMR. While XPS analysis shows that the above procedure forms molecular

layers with exposed amine groups as depicted in Fig. 1, further insight into the specific chemical structures of the molecular ligands upon attachment is needed. We used ^{1}H NMR to characterize the functionalized NP surfaces, as shown in Fig. 3 and Table 1. While a detailed analysis of the NMR data is included in the Supporting Information, several important observations are noted here. We first note that vinyl protons, which would appear in the 5-6 ppm region, are not observed in any of the five spectra shown in Fig. 3. This result demonstrates that the terminal vinyl groups of the starting ligands have reacted in the course of above procedure and that the ligands are attached to the DNP surface through the vinyl terminus. Further confirmation of the chemical structure of the surface-attached molecules is obtained from a more detailed analysis of the spectra (Supporting Information S6). Table 1 summarizes the assignments and chemical species types for all peaks in the ^{1}H NMR spectra of the five amine-functionalized DNP surfaces. The ^{1}H-NMR data in Fig. 3 provide detailed structure confirmation that the five cationic surfaces have the chemical structures depicted in Figure 1. As described in the methods section, in order to help understand the roles of amino groups in controlling the biological impact and toxicity of cationic nanoparticles, we quantify the total concentration of amino groups for each DNP surfaces by integrating the areas of peaks characteristic of amine moieties (labeled in c, f, g, i, j, $l_{1\text{-}8}$, m, n and o). The measured concentrations of the amino groups in each stock samples are included in the Supporting Information, S6, Table S3. All functionalized DNP solutions were then diluted to the same amino group concentration for the bacterial exposure.

Table 1. Peak assignment for ^{1}H-NMR spectra of amine-functionalized DNP surfaces.

DNP surfaces	^{1}H δ (ppm)	Assignment	Type
C3-NH_3^+	0.8	a	-(CH_2)$_n$
	1.2	b	-(CH_2)$_n$
	2.03	c	-$CH_2NH_3^+$
C3-$N(CH_3)_3^+$	0.07-0.15	d-e	-(CH_2)$_n$
	3.1	g	-$N(CH_3)_3^+$
	3.9	f	-$CH_2N(CH_3)_3^+$
C11-$N(CH_3)_3^+$	1.33	$h_{1\text{-}10}$	-(CH_2)$_n$
	3.11	j	-$N(CH_3)_3^+$
	3.35	i	-$CH_2N(CH_3)_3^+$
TEPA	1.02-1.21	$k_{1\text{-}5}$	-(CH_2)$_n$
	3.46-3.66	$l_{1\text{-}8}$	-CH_2NH
			-CH_2NH_2
PAH	1.17	n	-CH_2
	1.59	o	-CH-CH_2
	2.67	m	-$CH_2NH_3^+$

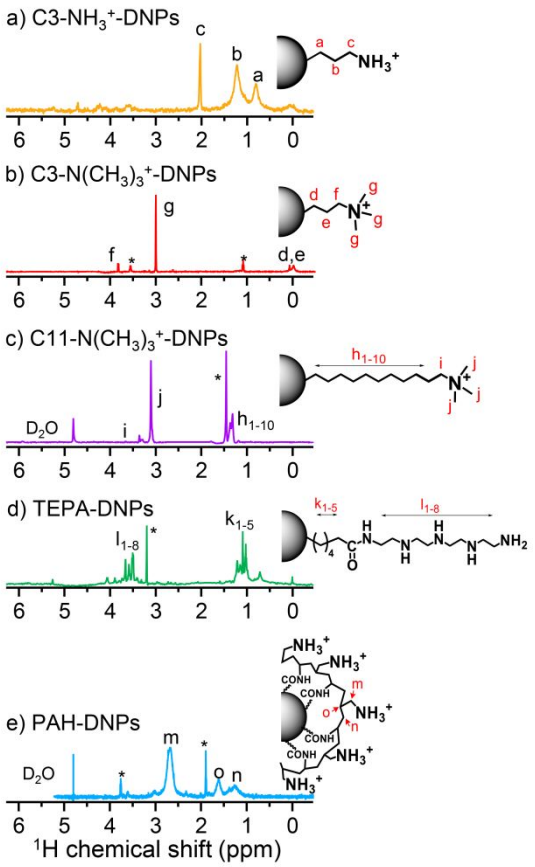

Figure 3. ^{1}H NMR spectra of a) C3-NH_3^+-DNPs, b) C3-$N(CH_3)_3^+$-DNPs c) C11-$N(CH_3)_3^+$-DNPs, d) TEPA-DNPs and e) PAH-DNPs. Asterisk denotes for solvent peaks.

Biological impact of cationic DNPs on *S. oneidensis*. ***Growth-based viability and Live/Dead assay.*** We examined the influence of the five different positively charged amine functionalized- DNPs on the Gram-negative bacterium *Shewanella oneidensis* MR-1 (*S. oneidensis*) using a growth-based viability assay.[33] Figure 4a shows viability of the *S. oneidensis* after introduction of functionalized DNPs for 1 h, reported for different concentration of surface-tethered amino groups. None of the DNPs functionalized with small molecule ligands (e.g., C3-$N(CH_3)_3^+$-DNPs, C3-NH_3^+-DNPs, C11-$N(CH_3)_3^+$-DNPs and TEPA-DNPs) have a significant negative influence on the viability of *S. oneidensis* over the concentration range studied; In contrast, the PAH-DNPs show significant toxicity even at low amine concentration of 10 nM (equivalent DNPs concentration: 0.4 mg/L), and induce 100% cell death at 20 nM amine concentration (DNPs: 0.8 mg/L) and above. To confirm that the toxicity is a nanoparticle surface-specific effect, we also conducted control studies exposing *S. oneidensis* to the free ligands. As shown in Fig. 4b, none of the ligands, including PAH, show any toxicity across the same amine concentration range. Thus, we conclude that the toxicity of PAH is only observed when it is attached to the DNPs and is therefore a "nanoparticle-surface-specific" effect. To understand the specific interactions that led to the high cytotoxicity, we employed the Live/Dead (L/D) assay to quantify the membrane integrity of the cells.[39-41] The L/D assay is a fluorescence-based method that uses two different

fluorescent dyes that bind to nucleic acid: green fluorescent SYTO® 9 and red fluorescent propidum iodide (PI) dyes.[42] These two stains have different abilities to penetrate healthy bacterial cells: the SYTO9 stain (excitation at 485 nm, emission at 528 nm) is membrane-permeant, whereas the PI stain (excitation at 485 nm, emission at 638 nm) only crosses damaged cell membranes. Figure 4c shows the influence of the five cationic-DNPs on the integrity of cell membranes of *S. oneidensis*, presented as ratios of fluorescence intensity of SYTO9 to PI stain that were exposed with NP-cells matrices. Because the signals from SYTO9 stain represents all cells and signals from PI stain represents only cells with damaged membranes, the fluorescence intensity ratio of SYTO9 to PI is related to the fraction of cells with intact membranes. The L/D assay exhibits the same trend as the GBV assay where the four DNPs functionalized with small-molecule ligands (C3-$N(CH_3)_3^+$-DNPs, C3-NH_3^+-DNPs, C11-$N(CH_3)_3^+$-DNPs and TEPA-DNPs) had almost no effect on the integrity of *S. oneidensis* membrane, while PAH-DNPs induce significant membrane damage (20% of all cells having damaged membranes) at 10 nM amine concentration (DNPs: 0.4 mg/L) and up to 60 % membrane damage at higher amine concentration (Fig. 4c).

The results from the L/D control studies using free ligands (Fig. 4d) are consistent with the results of GBV measurements, showing that none of the free ligands (including PAH) induce significant membrane damage across the same concentration range, while the covalently linked PAH polymer induces membrane damage when attached to DNP surface. The reduced viability revealed by the GBV assay and the membrane damage revealed by the L/D assays demonstrate that amino groups present in an amino-containing polymer (such as PAH) induce much strong biological interactions compared with the same concentration of primary or quaternary amino groups that are tethered more closely to the DNP surfaces (such as linear ligands with terminal amino groups). We further note that if we had instead presented these data as a function of nanoparticle concentration instead of amino concentration, the strong interactions of PAH would be even more apparent because of the higher number of ligand density of PAH-NDPs per nanoparticle (Supporting Information S7). Prior studies have often correlated toxicity of nanoparticles with the presence of a net positive charge.[2, 13-15] However, recent studies using both experiments and MD simulations have suggested that, at high amine densities, both the total number of charged groups and the fraction of amine in a charged state can be less than those at intermediate coverages, due to Coulombic interactions between neighboring sites.[43-44] We measured the zeta potential (ζ potential) for all five cationic surfaces in both nanopure water and HEPES buffer as this is the biological exposure medium. Figure 4e shows that the ζ potential for the DNPs

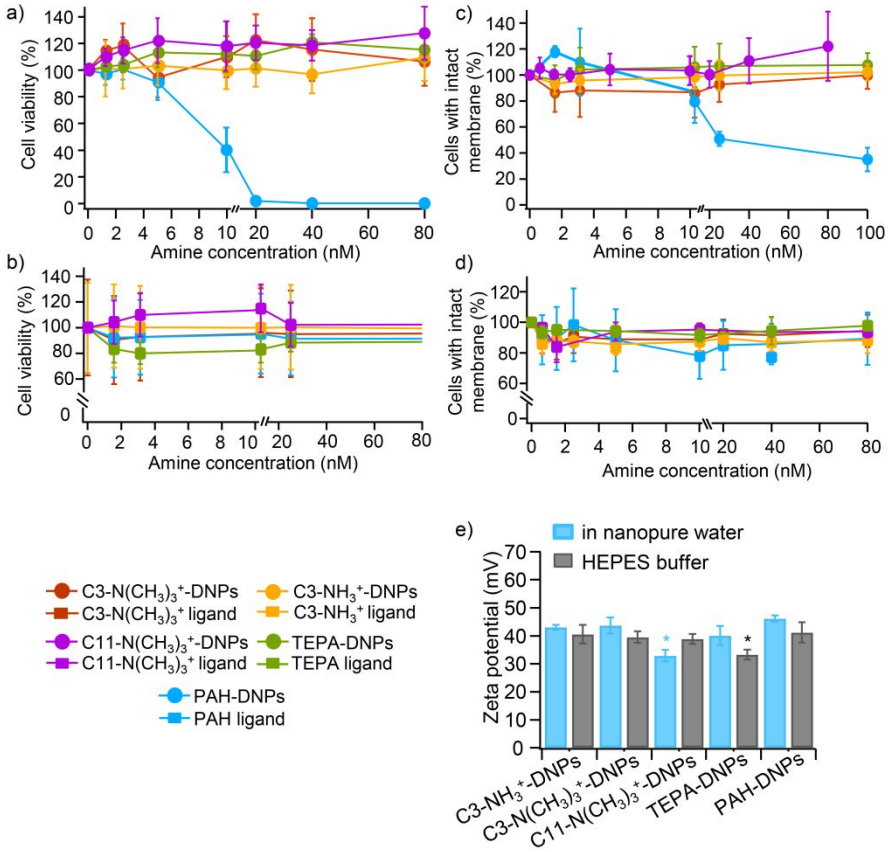

Figure 4. Growth-based viability results of *S. oneidensis* upon exposure to all cationic diamond nanoparticles (a) and free cationic ligands (b) (n = 4), the bacterial Live/Dead assay results assessing membrane integrity of *S. oneidensis* by all cationic DNPs (c), and free cationic ligands (d) (n = 6), and (e) ζ-potential values of all cationic DNPs in HEPES buffer (bacterial medium) (n > 5 from technical replicates). Asterisk denotes statistical differences among measurements using one-way ANOVA Tukey's multiple comparison test ($p < 0.05$). All error bars represent the standard deviation.

that are functionalized with linear small molecule ligands (C3-NH_3^+-DNPs, C3-$N(CH_3)_3^+$-DNPs, C11-$N(CH_3)_3^+$- DNPs and TEPA-DNPs) and the DNPs that are functionalized with polymer (PAH-DNPs) are statistically identical in ζ potential, except for TEPA-DNPs with slightly lower ζ potential. The previous molecular dynamics studies have shown that when the net surface charge density is sufficiently high, the zeta potential is only weakly dependent on the density of surface charges, due to charge compensation by the counter-ions. [45-47] In the present work, charge compensation by counter-ions likely plays a role in controlling the zeta potentials, such that the the multi-cationic PAH shows almost identical zeta potential as the mono-cationic molecular ligand at DNP surfaces. An important conclusion from this work is that the ζ potential alone is not a good parameter to predicting biological impact of functionalized nanoparticles. Overall, the GBV toxicity and L/D assay results show that the DNPs functionalized with the small linear molecules do not have any negative effect on the *S. oneidensis* viability or on membrane integrity, while the PAH-functionalized DNPs induce significant cell death and membrane damage even at lower concentrations. These results show that neither amine concentration nor the surface charge (measured by ζ potential) is the key factor in this difference; rather, the ligand conformation and spatial distribution of amino groups must be playing important roles in controlling the biological interactions.

Cell membrane deformation induced by polyamine functionalized DNPs. To determine the influence of functionalized DNPs on *S. oneidensis* cell membranes, we analyzed the structure of *S. oneidensis* cell membranes after exposure to functionalized DNPs using TEM. Since all four small-molecule ligand-functionalized DNPs show similar responses in GBV and L/D assay, we chose C3-$N(CH_3)_3^+$-DNPs as a representative linear ligand for comparison with PAH-DNPs. Figure 5a-b shows TEM images of untreated *S. oneidensis* cells in bright- field imaging mode. Figure 5c-d shows two representative TEM images of the bacterial cells after exposure to C3-$N(CH_3)_3^+$-DNPs; no major membrane distortion or disruption is visible, and the DNPs appear to be adhered to the outer layer of the cell membranes (indicated in red circle). In contrast, Figure 5e-f shows TEM image of the bacterial cells after exposure to PAH- DNPs; in this case, significant membrane distortion with spherical protrusions are observed on the outside of the bacterial membranes (indicated in red squares). These structures appear similar to previously reported images of outer membrane vesicles (OMVs).[48-50] Prior work has shown that OMVs can be formed as a stress response.[51] Similarly, the structures observed in our studies may be an indication of stress induced by PAH-DNPs. We have included additional TEM images at larger size in the Supporting Information S8. In summary, the TEM images in Fig. 5 demonstrate that the *S. oneidensis* cell surfaces respond much more strongly to the NPs functionalized with the polymer PAH compared with NPs functionalized with the linear small molecule ligand, even when the total concentration of amine groups is the same.

Role of molecular structure. Although the strong correlation between bacteria viability (Fig. 4a-b) and membrane damage (Fig. 4c-d and 5) was expected, our overall results are surprising in two ways. First, control experiments using the free PAH cationic polymer show that free PAH polymer does not induce membrane damage or decrease in cell viability across the tested amine concentrations. The cytotoxicity of PAH-DNPs only results from surface-attached PAH polymers. Second, both GBV and L/D assays show that on a "per amine" basis, each amino group of PAH-DNPs induces significantly higher toxicity than an equal number of amino groups on a linear small molecule ligand. Viability measurements normalized to

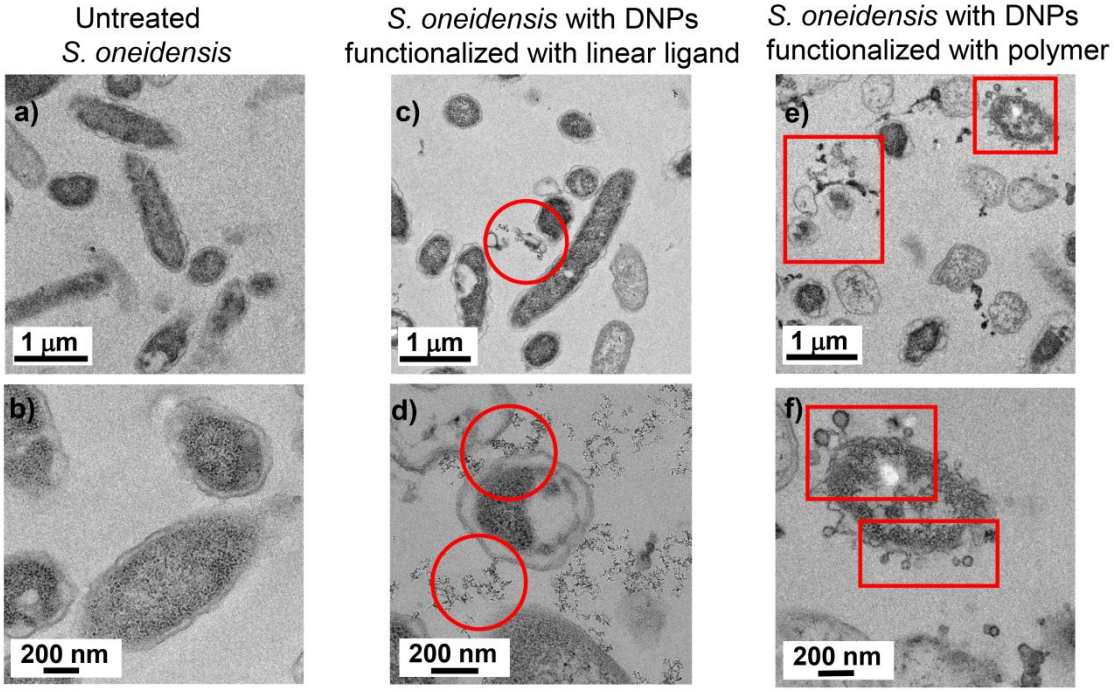

Figure 5. TEM images of (a-b) healthy *S. oneidensis* without exposure to cationic DNPs, (c-d) *S. oneidensis* after exposure to linear molecular ligand functionalized DNPs (C3-$N(CH_3)_3^+$-DNPs) and (e-f) *S. oneidensis* after exposure to polymer functionalized DNPs (PAH-DNPs). TEM images were taken using *S. oneidensis* that was treated with 80 nM amine concentration at DNP surfaces.

amino concentration (Fig. 4a-d) show that the concentration of surface-exposed amino groups in solution is not the key factor in this difference, nor is the zeta potential. Dielectrophoretic light-scattering estimates the zeta potential by measuring dielectrophoretic mobility and within using a model (such as the widely used Smoluchowski model[48, 51-53] to relate the measured mobility to a zeta potential. However, this approach assumes that particles are hard spheres with uniform charge distribution and does not account for lateral inhomogeneities across the NP surfaces or for more extended distribution of charge in the electric double layer.[54-55] Consequently, measurement of the zeta potentials of DNPs functionalized with molecules having different morphologies (e.g., linear ligands vs. polymer-linked) does not adequately represent the differences in spatial distribution of charge. Our results show that the spatial distribution of charge plays a key role in nanoparticle-membrane interactions. The main difference between DNPs functionalized with linear ligands (such as C3-NH_3^+-DNPs) and those modified with covalent-bonded polymers (PAH-DNPs) is the conformation of the surface molecules. Figure 6 represents a schematic illustration of functionalized DNPs interacting with a model LPS layer. For DNPs that are functionalized with short linear molecules, the charges are located in a thin shell at the periphery of the molecular monolayer, as shown in Fig. 6a. In contrast, DNPs that are functionalized with polymers have charges that extend further from the nanoparticle surface. In prior work, we characterized the molecular conformations of DNPs covalently bonded to PAH.[26] Our

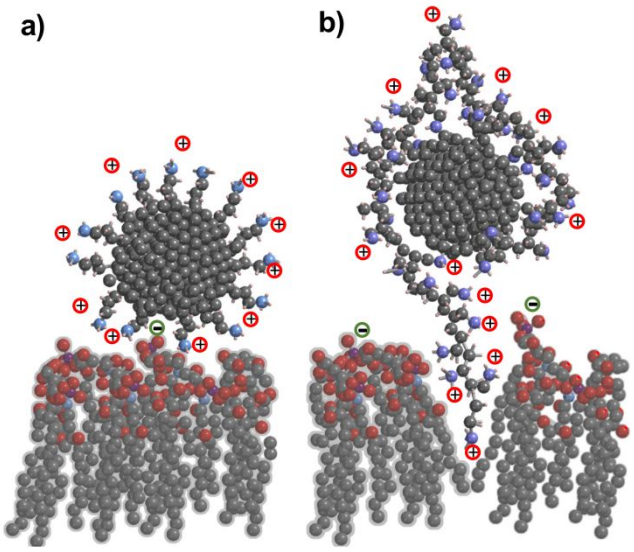

Figure 6. Conceptual illustration depicting spatial distribution of charge of DNPs functionalized with a) linear molecular ligands and b) covalently linked polymer interacting with a model LPS layer. While short molecular ligands interact only with the outermost regions of the LPS layers of the cellular membrane, loops and tails of the polymer can insert into the layers, leading to membrane disruption. Gray spheres represent C atoms; red O atoms; blue N atoms, purple P atoms of LPS. Positive charges correspond to amino groups; negative charges to phosphate groups of LPS.

NMR T_2 measurements showed that the PAH molecules exhibited two distinct populations, corresponding to sites bonded to the surface and other sites consisting of highly flexible polymer loops and tails. Similar conformations have been reported for other polymers at planar and nanoparticle surfaces.[56-60] The presence of loops and tails leads to an average charge distributed over a finite thickness adjacent to the DNP surfaces, extending the double-layer and increasing the hydrodynamic thickness. These effects are reflected in the larger hydrodynamic diameter (d_h=61.6 ± 2.2 nm) of DNPs modified with PAH compared with DNPs modified with linear ligands (d_h~30 nm). Other prior studies of polymer-modified nanoparticles have reported similar morphologies,[26, 59, 61] with loops and exposed tails extending into the adjacent liquid medium.[56, 58, 60] We propose that these loops and tails are largely responsible for the interaction of the PAH-NPs with *S. oneidensis* cell membranes. Specifically, we attribute the differential toxicity of PAH-ND and linear small molecule-functionalized DNPs to differences in the radial extent of the charged groups. Prior work[29] using molecular dynamics simulations has demonstrated that PAH binds to the LPS layer in Gram-negative bacteria through electrostatic interactions and eventually migrates to the core region of the LPS. Therefore, we propose that it is the larger radial extent of the loops and tails of the surface-linked PAH polymer enables penetration of the PAH (and its associated amino groups) into the lipopolysaccharide (LPS) layer at the surface of the Gram-negative *S. oneidensis* cell membrane. The positive charges allows the cationic NPs to bind to the surface of the bacterial membrane through electrostatic interactions, and the conformationally flexible PAH loops and tails assist physical insertion into the LPS layer.

CONCLUSIONS

These studies demonstrate that while cationic charged groups can enhance nanoparticle interaction with cellular membranes, the detailed molecular structure of the molecules, which controls the spatial distribution and presentation of charged groups, plays a key role. While nanoparticle charges are frequently characterized using the zeta potential, this single parameter does not fully capture the essential molecular aspects that control the nanoparticle interactions. Our work indicates that biological impact of cationic nanoparticles is greatest when the molecular functional groups extend away from the nanoparticle core in a flexible manner that can facilitate penetration of the molecules into the outermost molecular layers of the bacterial membrane. This work provides new perspectives on why cationic surface layers induce membrane damage in bacterial cells, and will facilitate further understanding of the fundamental mechanisms of cell membrane interactions of engineered NPs.

ASSOCIATED CONTENT

Supporting Information

Procedures of 11-trimethylamine-1-undecene bromide synthesis and characterization, details of DNPs functionalization conditions, hydrodynamic size and zeta

potential analysis of functionalized DNPs, XPS quantification of functionalized-DNPs, biological responses plot of *S. oneidensis* versus NP concentration and additional TEM images of NP-exposed *S.oneidensis*.

The Supporting Information is available free of charge on the ACS Publications website.

AUTHOR INFORMATION

Corresponding Author

* Robert J. Hamers, rjhamers@wisc.edu

ORCID

Yongqian Zhang: 0000-0001-9637-5314

Natalie V. Hudson-Smith: 0000-0002-2642-0711

Meghan Cahill: 0000-0002-1514-7625

Z. Vivian Feng: 0000-0002-3329-3781

Christy L. Haynes: 0000-0002-5420-5867

Robert J. Hamers: 0000-0003-3821-9625

Present Addresses

§ Department of Chemistry, Lawrence University, Appleton, Wisconsin, 54911, United States.

Author Contributions

The manuscript was written through contributions of all authors.

Funding Sources

National Science Foundation, CHE-1503408
National Science Foundation, 00039202
National Science Foundation, DMR-1720415
National Institutes of Health, S10OD012245

ACKNOWLEDGMENT

This work was supported by the National Science Foundation under the Center for Sustainable Nanotechnology, CHE-1503408. The CSN is part of the Centers for Chemical Innovation Program. N. Hudson-Smith acknowledges support through the National Science Foundation Graduate Research Fellowship Program (00039202). XPS studies used facilities and instrumentation supported by NSF through the University of Wisconsin Materials Research Science and Engineering Center (DMR-1720415). The Bruker Avance 600 NMR instrument used in this work was supported by the National Institutes of Health grants S10OD012245. Parts of this work were carried out in the Characterization Facility, University of Minnesota, which receives partial support from NSF through the MRSEC program.

ABBREVIATIONS

DNPs, diamond nanoparticles; XPS, x-ray photoelectron spectroscopy; NMR, nuclear magnetic resonance; PAH, poly(allylamine hydrochloride)

REFERENCES

1. Klaine, S. J.; Alvarez, P. J. J.; Batley, G. E.; Fernandes, T. F.; Handy, R. D.; Lyon, D. Y.; Mahendra, S.; McLaughlin, M. J.; Lead, J. R., Nanomaterials in the environment: Behavior, fate, bioavailability, and effects. *Environ. Toxicol. Chem.* **2008,** *27*, 1825-1851.
2. Verma, A.; Stellacci, F., Effect of surface properties on nanoparticle–cell interactions. *Small* **2010,** *6*, 12-21.
3. Fleischer, C. C.; Payne, C. K., Nanoparticle Surface Charge Mediates the Cellular Receptors Used by Protein-Nanoparticle Complexes. *J. Phys. Chem. B* **2012,** *116*, 8901-8907.
4. Albanese, A.; Tang, P. S.; Chan, W. C. W., The effect of nanoparticle size, shape, and surface chemistry on biological systems. *Ann. Rev. Biomed. Engr.* **2012**, *14*, 1-16.
5. Cho, E. C.; Xie, J. W.; Wurm, P. A.; Xia, Y. N., Understanding the role of surface charges in cellular adsorption versus internalization by selectively removing gold nanoparticles on the cell surface with a I_2/KI etchant. *Nano Lett.* **2009,** *9*, 1080-1084.
6. Setyawati, M. I.; Mochalin, V. N.; Leong, D. T., Tuning endothelial permeability with functionalized nanodiamonds. *ACS Nano* **2016,** *10*, 1170-1181.
7. Silva, T.; Pokhrel, L. R.; Dubey, B.; Tolaymat, T. M.; Maier, K. J.; Liu, X. F., Particle size, surface charge and concentration dependent ecotoxicity of three organo-coated silver nanoparticles: Comparison between general linear model-predicted and observed toxicity. *Sci. Total Environ.* **2014,** *468*, 968-976.
8. Verma, A.; Uzun, O.; Hu, Y.; Hu, Y.; Han, H.-S.; Watson, N.; Chen, S.; Irvine, D. J.; Stellacci, F., Surface-structure-regulated cell-membrane penetration by monolayer-protected nanoparticles. *Nat. Mater.* **2008,** *7*, 588.
9. Verma, A.; Arshad, F.; Ahmad, K.; Goswami, U.; Samanta, S. K.; Sahoo, A. K.; Sk, M. P., Role of surface charge in enhancing antibacterial activity of fluorescent carbon dots. *Nanotechnol.* **2020,** *31*, 9.
10. Huang, K.; Hu, Y.; Yu, C. J.; Boerhan, R.; Jiang, G. Q., Charged surface groups of nanoparticles and the adsorbed proteins codetermine the fate of nanoparticles upon interacting with cells. *Rsc Advances* **2016,** *6*, 58315-58324.
11. Mensch, A. C.; Hernandez, R. T.; Kuether, J. E.; Torelli, M. D.; Feng, Z. V.; Hamers, R. J.; Pedersen, J. A., Natural organic matter concentration impacts the interaction of functionalized diamond nanoparticles with model and actual bacterial membranes. *Environmental science & technology* **2017,** *51*, 11075-11084.
12. Feng, Z. V.; Gunsolus, I. L.; Qiu, T. A.; Hurley, K. R.; Nyberg, L. H.; Frew, H.; Johnson, K. P.; Vartanian, A. M.; Jacob, L. M.; Lohse, S. E., Impacts of gold nanoparticle charge and ligand type on surface binding and toxicity to Gram-negative and Gram-positive bacteria. *Chem. Sci.* **2015,** *6*, 5186-5196.
13. Goodman, C. M.; McCusker, C. D.; Yilmaz, T.; Rotello, V. M., Toxicity of gold nanoparticles functionalized with cationic and anionic side chains. *Bioconjugate chemistry* **2004,** *15*, 897-900.
14. Arvizo, R. R.; Miranda, O. R.; Thompson, M. A.; Pabelick, C. M.; Bhattacharya, R.; Robertson, J. D.; Rotello, V. M.; Prakash, Y.; Mukherjee, P., Effect of nanoparticle surface charge at the plasma membrane and beyond. *Nano Lett.* **2010,** *10*, 2543-2548.
15. Fleischer, C. C.; Payne, C. K., Nanoparticle–cell interactions: molecular structure of the protein corona and cellular outcomes. *Accounts of chemical research* **2014,** *47*, 2651-2659.
16. Hong, S.; Leroueil, P. R.; Janus, E. K.; Peters, J. L.; Kober, M.-M.; Islam, M. T.; Orr, B. G.; Baker Jr, J. R.; Banaszak Holl, M. M., Interaction of polycationic polymers with supported lipid bilayers and cells: nanoscale hole formation and enhanced membrane permeability. *Bioconjugate chemistry* **2006,** *17*, 728-734.
17. Giljohann, D. A.; Seferos, D. S.; Patel, P. C.; Millstone, J. E.; Rosi, N. L.; Mirkin, C. A., Oligonucleotide loading determines cellular uptake of DNA-modified gold nanoparticles. *Nano Lett.* **2007,** *7*, 3818-3821.
18. Herbig, M. E.; Assi, F.; Textor, M.; Merkle, H. P., The cell penetrating peptides pVEC and W2-pVEC induce transformation of gel phase domains in phospholipid bilayers without affecting their integrity. *Biochemistry* **2006,** *45*, 3598-3609.

19. Perera, G. S.; Athukorale, S. A.; Perez, F.; Pittman, C. U.; Zhang, D., Facile displacement of citrate residues from gold nanoparticle surfaces. *J. Coll. Interfac. Sci.* **2018,** *511*, 335-343.

20. Stobiecka, M.; Deeb, J.; Hepel, M., Ligand exchange effects in gold nanoparticle assembly induced by oxidative stress biomarkers: Homocysteine and cysteine. *Biophys. Chem.* **2010,** *146*, 98-107.

21. Ackerson, C. J.; Sykes, M. T.; Kornberg, R. D., Defined DNA/nanoparticle conjugates. *Proc. Nat. Acad. Sci. USA* **2005,** *102*, 13383-13385.

22. Yang, W.; Auciello, O.; Butler, J. E.; Cai, W.; Carlisle, J. A.; Gerbi, J. E.; Gruen, D. M.; Knickerbocker, T.; Lasseter, T. L.; Russell, J. N.; Smith, L. M.; Hamers, R. J., DNA-modified nanocrystalline diamond thin-films as stable, biologically active substrates. *Nat. Mater.* **2002,** *1*, 253-257.

23. Stavis, C.; Clare, T. L.; Butler, J. E.; Radadia, A. D.; Carr, R.; Zeng, H.; King, W. P.; Carlisle, J. A.; Aksimentiev, A.; Bashir, R.; Hamers, R. J., Surface functionalization of thin-film diamond for highly stable and selective biological interfaces. *Proc. Nat. Acad. Sci. USA s* **2011,** *108*, 983-988.

24. Krueger, A.; Lang, D., Functionality is key: recent progress in the surface modification of nanodiamond. *Adv. Func. Mater.* **2012,** *22*, 890-906.

25. Zhang, Y.; Abbaspour Tamijani, A.; Taylor, M. E.; Zhi, B.; Haynes, C. L.; Mason, S. E.; Hamers, R. J., Molecular surface functionalization of carbon materials via radical-induced grafting of terminal alkenes. *J. Am. Chem. Soc.* **2019,** *141*, 8277-8288.

26. Zhang, Y.; Fry, C. G.; Pedersen, J. A.; Hamers, R. J., Dynamics and morphology of nanoparticle-linked polymers elucidated by nuclear magnetic resonance. *Anal. Chem.* **2017,** *89*, 12399-12407.

27. Hau, H. H.; Gralnick, J. A., Ecology and biotechnology of the genus *Shewanella*. *Annu. Rev. Microbiol.* **2007,** *61*, 237-258.

28. Qiu, T.; Bozich, J.; Lohse, S.; Vartanian, A.; Jacob, L.; Meyer, B.; Gunsolus, I.; Niemuth, N.; Murphy, C.; Haynes, C., Gene expression as an indicator of the molecular response and toxicity in the bacterium *Shewanella oneidensis* and the water flea *Daphnia magna* exposed to functionalized gold nanoparticles. *Environ. Sci.: Nano* **2015,** *2*, 615-629.

29. Buchman, J. T.; Rahnamoun, A.; Landy, K. M.; Zhang, X.; Vartanian, A. M.; Jacob, L. M.; Murphy, C. J.; Hernandez, R.; Haynes, C. L., Using an environmentally-relevant panel of Gram-negative bacteria to assess the toxicity of polyallylamine hydrochloride-wrapped gold nanoparticles. *Environ. Sci.: Nano* **2018,** *5*, 279-288.

30. Vigderman, L.; Manna, P.; Zubarev, E. R., Quantitative replacement of cetyl trimethylammonium bromide by cationic thiol ligands on the surface of gold nanorods and their extremely large uptake by cancer cells. *Angew. Chem., Int. Ed.* **2012,** *51*, 636-641.

31. Williams, O. A.; Hees, J.; Dieker, C.; Jäger, W.; Kirste, L.; Nebel, C. E., Size-dependent reactivity of diamond nanoparticles. *ACS Nano* **2010,** *4*, 4824-4830.

32. Fairley, N., CasaXPS Version 2.3. 14. *Casa Software Ltd* **1999,** *2005*.

33. Qiu, T. A.; Nguyen, T. H. T.; Hudson-Smith, N. V.; Clement, P. L.; Forester, D.-C.; Frew, H.; Hang, M. N.; Murphy, C. J.; Hamers, R. J.; Feng, Z. V., Growth-based bacterial viability assay for interference-free and high-throughput toxicity screening of nanomaterials. *Anal. Chem.* **2017,** *89*, 2057-2064.

34. Strother, T.; Hamers, R. J.; Smith, L. M., Covalent attachment of oligodeoxyribonucleotides to amine-modified Si (001) surfaces. *Nucleic Acids Res.* **2000,** *28*, 3535-3541.

35. Ederer, J.; Janoš, P.; Ecorchard, P.; Tolasz, J.; Štengl, V.; Beneš, H.; Perchacz, M.; Pop-Georgievski, O., Determination of amino groups on functionalized graphene oxide for polyurethane nanomaterials: XPS quantitation vs. functional speciation. *RSC Adv.* **2017,** *7*, 12464-12473.

36. Baker, S. E.; Cai, W.; Lasseter, T. L.; Weidkamp, K. P.; Hamers, R. J., Covalently bonded adducts of deoxyribonucleic acid (DNA) oligonucleotides with single-wall carbon nanotubes: synthesis and hybridization. *Nano Lett.* **2002,** *2*, 1413-1417.

37. Bogdanowicz, R.; Sawczak, M.; Niedzialkowski, P.; Zieba, P.; Finke, B.; Ryl, J.; Karczewski, J.; Ossowski, T., Novel functionalization of boron-doped diamond by microwave pulsed-plasma polymerized allylamine film. *J. Phys. Chem. C* **2014,** *118*, 8014-8025.

38. Wang, X.; Ruther, R. E.; Streifer, J. A.; Hamers, R. J., UV-induced grafting of alkenes to silicon surfaces: photoemission versus excitons. *J. Am. Chem. Soc.* **2010,** *132*, 4048-4049.

39. Miller, J. S.; Quarles, J. M., Flow cytometric identification of microorganisms by dual staining with FITC and PI. *Cytometry:* **1990,** *11*, 667-675.

40. Lloyd, D.; Hayes, A. J., Vigour, vitality and viability of microorganisms. *FEMS Microbiol. Lett.***1995,** *133*, 1-7.

41. Bunthof, C. J.; van Schalkwijk, S.; Meijer, W.; Abee, T.; Hugenholtz, J., Fluorescent method for monitoring cheese starter permeabilization and lysis. *Appl. Environ. Microbiol.* **2001,** *67*, 4264-4271.

42. Mah, T.-F.; Pitts, B.; Pellock, B.; Walker, G. C.; Stewart, P. S.; O'Toole, G. A., A genetic basis for *Pseudomonas aeruginosa* biofilm antibiotic resistance. *Nature* **2003,** *426*, 306-310.

43. Zheng, Z.; Saar, J.; Zhi, B.; Qiu, T. A.; Gallagher, M. J.; Fairbrother, D. H.; Haynes, C. L.; Lienkamp, K.; Rosenzweig, Z., Structure–Property Relationships of Amine-rich and Membrane-Disruptive Poly (oxonorbornene)-Coated Gold Nanoparticles. *Langmuir* **2018,** *34*, 4614-4625.

44. Hong, J.; Hamers, R. J.; Pedersen, J. A.; Cui, Q., A hybrid molecular dynamics/multiconformer continuum electrostatics (MD/MCCE) approach for the determination of surface charge of nanomaterials. *J. Phys. Chem. C* **2017,** *121*, 3584-3596.

45. Manning, G. S., Counterion Condensation on Charged Spheres, Cylinders, and Planes. *J. Phys. Chem. B* **2007,** *111*, 8554-8559.

46. Manning, G. S., The Interaction between a Charged Wall and Its Counterions: A Condensation Theory. *J. Phys. Chem. B* **2010,** *114*, 5435-5440.

47. Dreier, L. B.; Nagata, Y.; Lutz, H.; Gonella, G.; Hunger, J.; Backus, E. H. G.; Bonn, M., Saturation of charge-induced water alignment at model membrane surfaces. *Science Advances* **2018,** *4*, eaap7415.

48. Subramanian, P.; Pirbadian, S.; El-Naggar, M. Y.; Jensen, G. J., Ultrastructure of *Shewanella oneidensis* MR-1 nanowires revealed by electron cryotomography. *Proce. Nat. Acad. Sci. USA* **2018,** *115*, E3246-E3255.

49. Pirbadian, S.; Barchinger, S. E.; Leung, K. M.; Byun, H. S.; Jangir, Y.; Bouhenni, R. A.; Reed, S. B.; Romine, M. F.; Saffarini, D. A.; Shi, L.; Gorby, Y. A.; Golbeck, J. H.; El-Naggar, M. Y., *Shewanella oneidensis* MR-1 nanowires are outer membrane and periplasmic extensions of the extracellular electron transport components. *Proc. Nat. Acad. Sci. USA* **2014,** *111*, 12883-12888.

50. Perez-Cruz, C.; Carrion, O.; Delgado, L.; Martinez, G.; Lopez-Iglesias, C.; Mercade, E., New type of outer membrane vesicle produced by the Gram-negative bacterium *Shewanella vesiculosa* M7(T): Implications for DNA content. *Appl. Environ. Microbiol.* **2013,** *79*, 1874-1881.

51. Schwechheimer, C.; Kuehn, M. J., Outer-membrane vesicles from Gram-negative bacteria: biogenesis and functions. *Nat. Rev. Microbiol.* **2015,** *13*, 605-619.

52. Hiemenz, P.; Rajagopalan, R., Electrophoresis and other electrokinetic phenomena. *Principles of colloid and surface chemistry* **1977,** *3*, 544-547.

53. Hunter, R. J., *Zeta potential in colloid science: principles and applications*. Academic press: 2013.

54. Feick, J. D.; Velegol, D., Electrophoresis of spheroidal particles having a random distribution of zeta potential. *Langmuir* **2000,** *16*, 10315-10321.

55. Feick, J. D.; Velegol, D., Measurements of charge nonuniformity on polystyrene latex particles. *Langmuir* **2002,** *18*, 3454-3458.

56. Blum, F. D., Magnetic resonance of polymers at surfaces. *Colloids and surfaces* **1990,** *45*, 361-376.

57. Claesson, P. M.; Dahlgren, M. A.; Eriksson, L., Forces between polyelectrolyte-coated surfaces: relations between surface interaction and floc properties. *Colloids and Surfaces A: Physicochemical and Engineering Aspects* **1994,** *93*, 293-303.

58. Cosgrove, T.; Griffiths, P.; Lloyd, P., Polymer adsorption. The effect of the relative sizes of polymer and particle. *Langmuir* **1995,** *11*, 1457-1463.

59. Lin, W.-Y.; Blum, F. D., Segmental dynamics of bulk and silica-adsorbed poly (methyl acrylate)-d_3 by deuterium NMR: the effect of molecular weight. *Macromolecules* **1998,** *31*, 4135-4142.

60. Hershkovits, E.; Tannenbaum, A.; Tannenbaum, R., Polymer adsorption on curved surfaces: a geometric approach. *J. Phys. Chem. C* **2007,** *111*, 12369-12375.

61. Blum, F. D.; Xu, G.; Liang, M.; Wade, C. G., Dynamics of Poly (vinyl acetate) in Bulk and on Silica. *Macromolecules* **1996,** *29*, 8740-8745.

Table of contents figure for publication only